Automated Ice Detection for Autonomous Underwater Gliders

Amy Phung*†, Gideon Billings§, Ted Maksym*, and Richard Camilli*
*Woods Hole Oceanographic Institution, Woods Hole, MA
†Massachusetts Institute of Technology, Cambridge, MA
§Australian Centre for Robotics, The University of Sydney, Sydney NSW 2006, Australia

***Abstract*—Autonomous underwater vehicles (AUVs) and gliders (AUGs) face significant operational challenges in ice-covered regions due to the need for periodic surfacing to transmit data, update position estimates, and facilitate recovery. In these environments, vehicles can become trapped, crushed, or displaced by currents or drifting ice. While large-scale distribution of sea ice and available open water can be detected via satellite imaging, it is not practical to communicate this information in a timely manner to underwater vehicles while submerged. Smaller, meter-scale ice fragments can pose significant risks to vehicle survivability but are beyond the spatial and temporal resolution capabilities of earth observing satellites. In this work, we describe an automated ice detection method using data collected by an AUG equipped with an upward-facing Mechanically Scanned Imaging Sonar (MSIS). We demonstrate the efficacy of this approach with results from field data collected in the Arctic marginal ice zone (MIZ).**

***Index Terms*—Autonomous underwater glider, marginal ice zone, operational robustness, sonar**

I. Introduction

The subsurface polar oceans are among the most poorly observed regions of the world's oceans, largely because of the logistical challenges of operating in ice-covered waters. However, the Arctic and Antarctic are among the fastest changing regions on earth, with rapid loss of sea ice and ocean warming having substantial implications for polar ecosystems, coastal communities, and ocean circulation and energy exchange. Although existing methods for large-scale ice measurements rely primarily on data collected by satellites, observations under sea ice and ice shelves provide additional context beyond remote sensing data, which are critical to understanding the coupled processes and feedback loops of ice-ocean-atmosphere interactions.

Autonomous Underwater Vehicles (AUVs) and Gliders (AUGs) have the potential to greatly expand our ability to monitor below the surface of ice-covered oceans, both spatially and temporally. However, AUVs and AUGs are subject to unique challenges operating under ice, as they require periodic surfacing to transmit data, update position estimates, and receive mission plans. When operating in these regions, vehicles risk being trapped beneath ice, crushed between ice floes, or lost due to currents affecting vehicle navigation relative to ice or wind, and currents driving the ice motion relative to the vehicle. These factors make it essential to have a temporally accurate understanding of ice distribution and dynamics in the vicinity of surfacing locations, to minimize mission risk and maximize vehicle survivability. Although remote sensing data can be used to plan operations to a limited degree, they cannot be readily used to guide underwater vehicles during a dive mission due to the challenges of underwater communication and navigation. To date, most AUV or AUG missions under ice have been relatively short in range and duration, where these conditions can be observed directly [1, 2], required external navigation beacons [3] or high-accuracy inertial navigation systems (INS) [4] for longer range under-ice operation, or were conducted near the ice edge when operating under ice shelves without the benefit of acoustic beacons or high-accuracy INS [5, 6].

Prior works have explored ice-based and seafloor-based navigation methods using a Doppler velocity log (DVL) to constrain navigation error and ice edge uncertainty [7, 8]. Additional methods such as iterative probing for ice leads [9] and rapid descent sequences to escape entrapment [4, 10] have been developed as countermeasures. However, these approaches are risky and inefficient. A more reliable solution for extending mission range and duration in areas with temporally and spatially varying ice coverage is for the vehicle to accurately characterize ice coverage before attempting a surfacing or evasive maneuver.

In this work we describe an automated process using a mechanically scanned imaging sonar (MSIS) for in-situ ice detection, estimation, and tracking, which we demonstrate onboard an AUG with minimal power and computational requirements. Data collected using this method can offer valuable scientific insight to improve our understanding of ice dynamics and distribution, while also contributing to operational safety by improving vehicle survivability in ice-prone environments.

II. Methods

MSIS sonars mechanically rotate a single narrow-beam transducer to map the environment, and can be used to detect

This research was supported through National Science Foundation Navigating the New Arctic Grant #1839063, National Ocean Partnership Program Grant #NA19OAR0110408, and the US Department of Energy's Office of Energy Efficiency and Renewable Energy program DE-EE0009801. A. Phung would like to acknowledge financial support from the National Science Foundation Graduate Research Fellowship (No. 2141064), and from the National Aeronautics and Space Administration (NASA) through the FINESST program (No. 80NSSC23K1391).

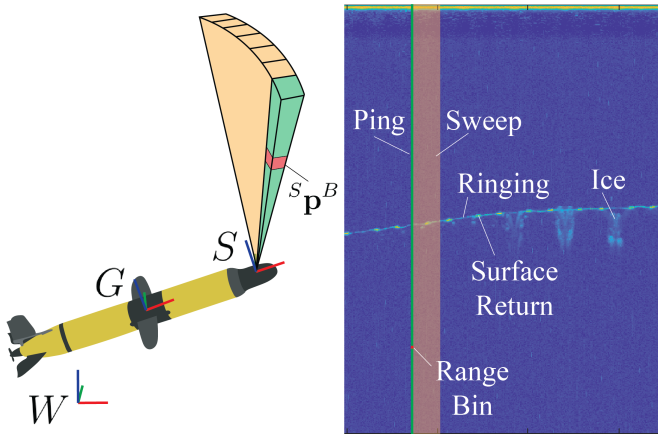

Fig. 1. (left) Diagram illustrating key coordinate frames and the MSIS configuration used for automated ice detection. (right) Unprocessed ping ensemble data with ice present.

ice coverage when the AUG is within the acoustic scanning range of the surface. In the implementation described here, the frequency is centered at 700MHz, providing a maximum range of approximately 75m. Data from this sensor is recorded as a ping ensemble, where each ping records intensity values for a series of range bins. Although the sonar can be configured to rotate across the entire 360° range, the sonar is configured with an upward looking range within ± 20° for surface ice characterization. We define a "sweep" as a set of pings from $-20°$ to $+20°$, as illustrated in Figure 1.

Each ping is first preprocessed to remove ringing caused by the acoustic return from the surface using the process described by Alg. 1. Given the ping ensemble P (stored as an $r \times n$ matrix, where r is the number of range bins and n are the number of pings in the dataset) and corresponding vehicle depth values (from pressure sensor data), this process computes the filtered ping ensemble $\bar{P}$ which contains the intensity data with the surface returns removed (Figure 2). For each ping angle, the surface return is characterized with the median value across the windowed data centered on the surface range bin. This median value is subtracted from the windowed data to remove the surface return.

After preprocessing, a dynamic threshold is used to identify and label discrete ice floes in the filtered data based on the backscatter peak shape and intensity, based on [11], and using the process described in Alg. 2. This threshold is set at one standard deviation above the median intensity value in the filtered ping ensemble $\bar{P}$. A dataset mask M is created to identify range bins where the recorded intensity exceeds this threshold. To filter out isolated high-intensity bins while preserving the ice structures in the data, an opening operation (erosion followed by dilation) is applied to M. The filtered result is denoted as $\bar{M}$. Ice is classified as a discrete entity if each sequential sweep contains at least one ice return in $\bar{M}$. These discrete labels are stored in C.

The filtered ping ensemble $\bar{P}$ and corresponding ice cluster labels C can be fused with vehicle location and pose estimates

Algorithm 1 Data Preprocessing

Input
P: Ping ensemble ($r \times n$ matrix)
D: Ping depths ($1 \times n$ row vector)
w: Window size
Output
$\bar{P}$: Filtered ping ensemble ($r \times n$ matrix)

B_s = LOOKUPSURFACEBIN(D)
$P_w = P[B_s - w : B_s + w, :]$ ▷ Windowed data around surface
for each ping angle θ **do**
  $P_\theta = \{p \in P_w | \text{PINGANGLE } (p) = \theta\}$
  $\mathbf{m}$ =MEDIAN $(P_\theta, \text{axis} = 1)$
  for each ping $p \in P_\theta$ **do**
    $\bar{p} = p[b_s - n : b_s + n] - \mathbf{m}$
    $\bar{P}_\theta = \bar{P}_\theta \cup \{\bar{p}\}$
  end for
  $\bar{P}_w = \bar{P}_w \cup \{\bar{P}_\theta\}$
end for
$\bar{P} = P$ ▷ Initialize output
$\bar{P}[B_s - n : B_s + n, :] = \bar{P}_w$ ▷ Apply windowed data to output

Algorithm 2 Ice Segmentation

Input
$\bar{P}$: Filtered ping ensemble ($r \times n$ matrix)
Output
$\bar{M}$: Filtered ice mask ($r \times n$ matrix)
C: Labeled Ice Clusters ($1 \times n$ row vector)

m = MEDIAN $(\bar{P})$
σ = STANDARDDEVIATION $(\bar{P})$
$M = \bar{P} > m + \sigma$
SE = STRUCTURINGELEMENT (disk, 2)
$\bar{M}$ = ERODE (M, SE)
$\bar{M}$ = DILATE $(\bar{M}, SE)$
C = LABELCLUSTERS $(\bar{M})$

to characterize ice coverage. Each range bin within the ice cluster can be projected to world coordinates as follows:

$$^W\mathbf{p}^B = {}^W\mathbf{X}^G {}^G\mathbf{X}^S {}^S\mathbf{p}^B \tag{1}$$

where $^W\mathbf{X}^G$ is given by glider pose estimate, $^G\mathbf{X}^S$ is given by the sonar's known mounting location on the glider, and $^S\mathbf{p}^B$ is the cartesian location of the range bin in the sonar's coordinate frame. The range bins are defined by r, θ, and can be written as:

$$^S\mathbf{p}^B = < r\sin(\theta), 0, r\cos(\theta) > \tag{2}$$

A 3D alphashape can be computed for each set of georeferenced points corresponding to the discrete ice floes to estimate their shape and volume.

III. RESULTS

Although this sea ice detection method is agnostic to the vehicle platform, we demonstrate its viability using the EPIC-

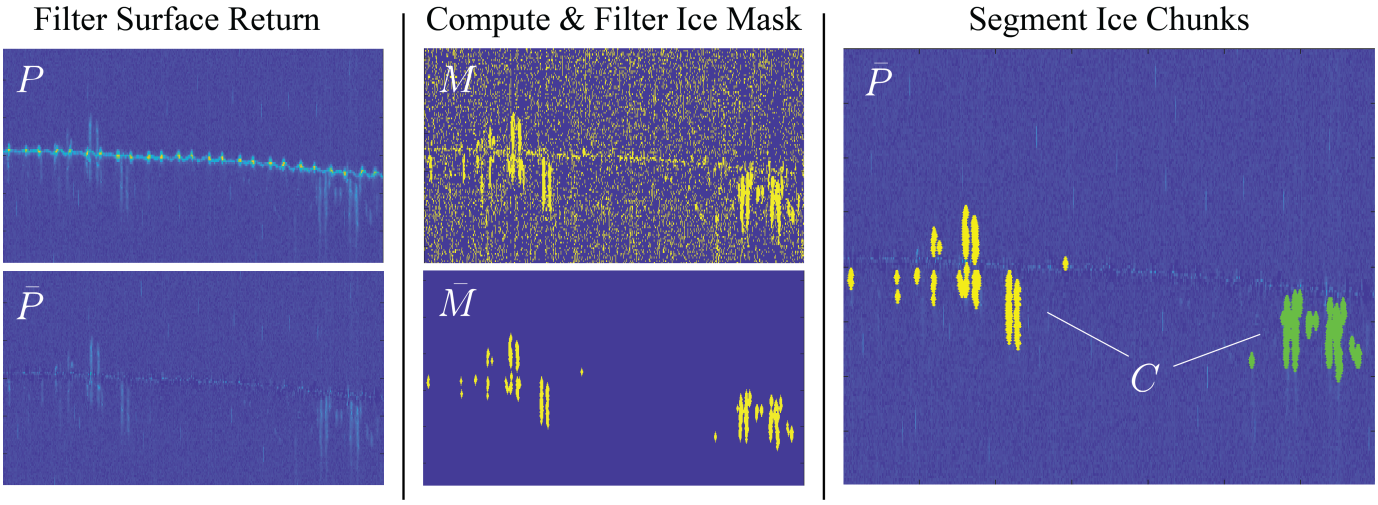

Fig. 2. Data filtering and ice segmentation pipeline. The original data P is filtered to remove the surface return. A mask M is created to highlight intensity values greater than 1σ from the median in the filtered data $\bar{P}$. An erosion-dilation process is applied to M to identify ice structures, which are segmented into discrete ice floes.

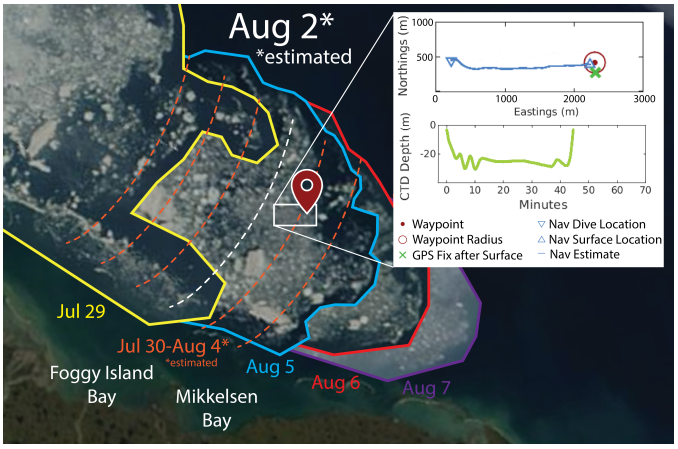

Fig. 3. Dataset collection area, overlaid on imagery from the NASA Worldview application [13]. The drift ice near the areas of operation are visualized as a time series composite image based on true color data from Terra/MODIS data [14] on July 29th and from August 5-7th, for reference. (Ice imagery is not available July 30th-August 4th due to cloud cover). (top inset) Dataset collection trajectory and dive profile.

DAUG vehicle. This Slocum G3 AUG, which has been modified for increased range while operating in water depths from 10 to 1000 m, is equipped with a passively pitch-stabilized Tritech Micron MSIS scanning radially about the vehicle's forward axis from within the nose-cone [12]. The method is demonstrated on a 2 km-long dataset collected in the Arctic MIZ during field trials in the Beaufort Sea on August 2nd, 2023.

Figure 4 illustrates the results generated by applying the sea ice detection method to the dataset. Several discrete ice floes are visible in the recorded MSIS data (Figure 4b). Based on this analysis, we estimate the percent ice cover in the testing region to be approximately 17%.

IV. Discussion

This ice detection and characterization method can be applied in operational scenarios to track the presence, thickness, and percent ice cover within a given region. Prior receiver operating characteristic (ROC) curve analysis [11] demonstrated that single-ping MSIS-based ice detection can provide a 76.8% true positive rate (TPR) and 17.5% false positive rate (FPR). However, with an ensemble of 10 successive pings, the TPR increases to 90.1% while the FPR remains relatively similar at 18.6%. The computational efficiency and relative accuracy of this acoustic ice detection process can potentially be used as an embedded real-time process to identify ice-free surface locations. This capability has the potential to reduce the dependence on transiting to previously identified safe surfacing locations. By extension, this capability relaxes georeferenced navigation accuracy requirements and may enable operation in regions with highly dynamic ice movement.

The real-time ability to characterize ice metrics such as size, shape, and percent coverage significantly reduces data transmission requirements by avoiding the need to transmit the full complement of raw data. This onboard perception and abstraction can reduce the required volume, time, and power for data transmission by approximately four orders of magnitude [15], potentially enabling periodic short-burst transmission of ice metrics using low bandwidth telemetry, such as through-water underwater acoustics while the AUG is still in mission. For high-risk and long-term unattended missions, periodic data offload is a useful method for preventing total data loss in the event of vehicle loss. Mission scenarios may include operations without icebreaker support during seasonal ice advance, or in extreme weather. The extended mission duration capability of the EPIC-DAUG vehicle could be used for loitering surveys, enabling continuous observation of regions that would otherwise have temporal gaps in Earth observing satellite (EOS) coverage. For example, the August 2,

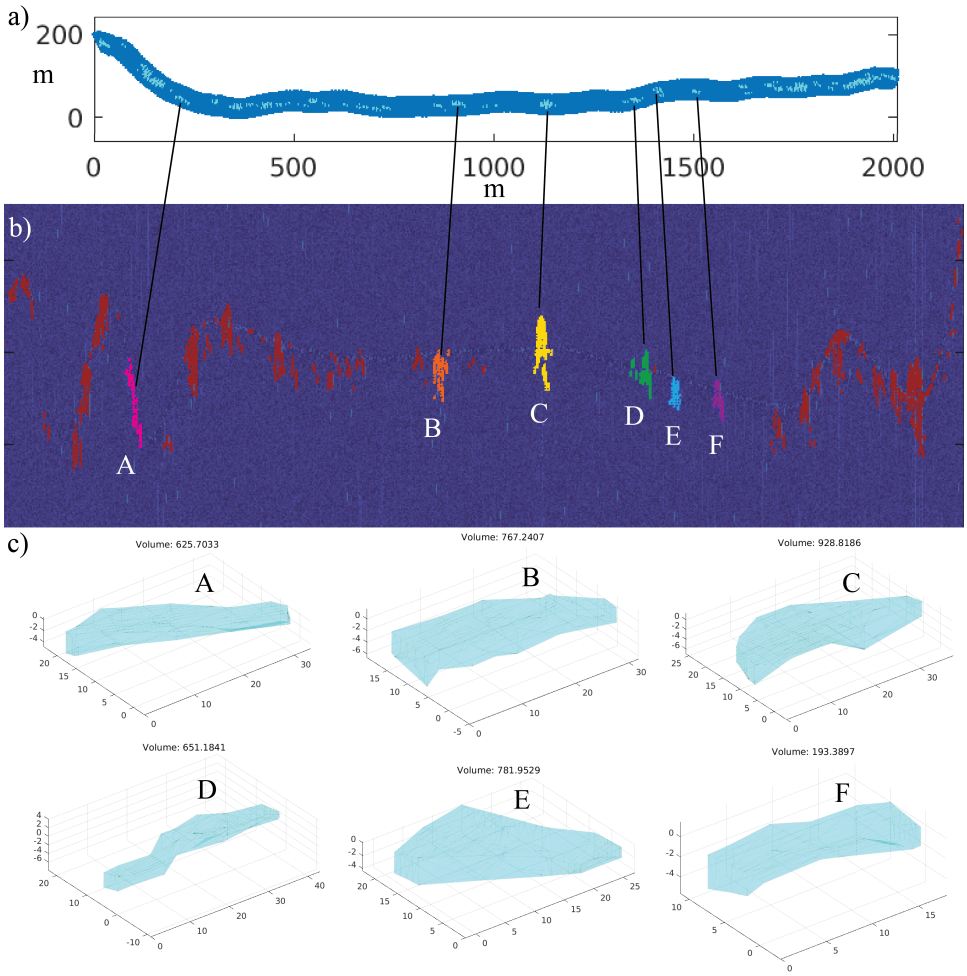

Fig. 4. (a) Georeferenced ice detections along glider trajectory (b) Raw MSIS data, with ice detections highlighted in red. Six representative ice floes are highlighted in a variety of colors. (c) 3D reconstructions of the six ice floes highlighted in b, with their respective estimated volume displayed in m^3.

2023 survey was completed during a Terra/MODIS coverage gap due to cloud cover between July 30 and August 4, as shown in Figure 3. Along with increased temporal resolution, the demonstrated ability of this acoustic method to characterize the shapes and volumes of ice floes at meter-scales (illustrated in Figure 4) extends the spatial resolution an order of magnitude lower than what is currently possible using high-resolution EOS ice observation [16]. This increased resolution is useful for generating a probabilistic estimate of surfacing risk based on percent ice coverage and characteristic keel depth. Increased observational resolution is also useful for a variety of geophysical studies, including more accurate ice inventory assessment, as well as improved understanding of the dynamics of wind and wave energy transfer influencing ice advection, breakup, and melt, and air-ice-ocean heat exchange. Computation and communications requirements suggest that a light-weight embedded architecture, using as an ARM processor or similarly low powered processor would provide sufficient capability to enable operation for extended under-ice survey missions.

At present, the survey method's $\pm$ 20° swath width limits the observable ice floe width to a maximum of 51m when operating at the sonar's maximum 75m range (with vehicle depth at 70m). This observational swath width decreases, with decreasing vehicle depth. For the August 2, 2023 survey, which was conducted at approximately 25m water depth, the swath width was limited to 18m. In cases where an ice floe extends beyond the width of the sonar swath, the ice measurement would be truncated, causing the observations to appear elongated (i.e., fully observed along-track, but truncated across-track). Possible corrections for this artifact may be to extend the sweep angle and thereby widen the swath width, or by assuming random orientation of the ice and applying a correction based on the estimated unobserved portions of the larger floes.

V. Conclusion

Although surfacing is essential for AUGs and low power AUVs to establish radio communications and constrain dead reckon navigation uncertainty, it is a risky operation in ice-covered regions. Dynamic ice cover presents a particularly challenging condition because the vehicle has little to no

access to timely remote sensing data (e.g., high-resolution EOS ice cover imagery). This presents a race condition, wherein the vehicle must obtain temporally accurate estimates of ice-free areas that are safe for surfacing and arrive at the surfacing location before conditions change. This sonar-based perception method demonstrates the capability for in-situ characterization of sea-ice coverage from an AUG for assessment of conditions for safe surfacing. This capability is not dependent on prior information, such as previously identified surfacing locations, or on contemporaneous external information provided by beacons or remote sensing updates. In addition to its utility for safe surfacing, the sonar-based perception process provides an efficient method to derive scientifically useful information such as ice-covered fraction, ice volume, and floe size distribution. Our ongoing work seeks to integrate this perception process within an embedded mission controller to inform opportunistic surfacing during long-range surveys within ice-covered regions.

References

[1] G. Williams, T. Maksym, J. Wilkinson, C. Kunz, C. Murphy, P. Kimball, and H. Singh, "Thick and deformed antarctic sea ice mapped with autonomous underwater vehicles," *Nature Geoscience*, vol. 8, no. 1, pp. 61–67, 2015.

[2] C. M. Lee, J. Thomson, M. I. Zone, and A. S. S. Teams, "An autonomous approach to observing the seasonal ice zone in the western arctic," *Oceanography*, vol. 30, no. 2, pp. 56–68, 2017.

[3] S. E. Webster, L. E. Freitag, C. M. Lee, and J. I. Gobat, "Towards real-time under-ice acoustic navigation at mesoscale ranges," in *2015 IEEE International Conference on Robotics and Automation (ICRA)*, pp. 537–544, IEEE, 2015.

[4] A. B. Phillips et al., "Autosub 2000 under ice: Design of a new work class auv for under ice exploration," in *2020 IEEE/OES Autonomous Underwater Vehicles Symposium (AUV)*, pp. 1–8, 2020.

[5] B. Allsup and Y. Wang, "Results from under ice antarctic glider operations at noc featuring new bsd systems," in *2024 International Underwater Glider Conference*, 2024.

[6] N. Krauzig et al., "New insights from a multi-glider survey on the ross sea continental shelf in antarctica," in *2024 International Underwater Glider Conference*, 2024.

[7] L. D. Barker and L. L. Whitcomb, "Performance analysis of ice-relative upward-looking doppler navigation of underwater vehicles beneath moving sea ice," *Journal of Marine Science and Engineering*, vol. 9, no. 2, p. 174, 2021.

[8] G. Billings, A. Phung, and R. Camilli, "Dvl-based odometry for autonomous underwater gliders," in *2023 IEEE/RSJ International Conference on Intelligent Robots and Systems (IROS)*, pp. 9910–9917, IEEE, 2023.

[9] C. Lee, H. Melling, H. Eicken, P. Schlosser, J.-C. Gascard, A. Proshutinsky, E. Fahrbach, C. Mauritzen, J. Morison, and I. Polykov, "Autonomous platforms in the arctic observing network," *Proceedings of Ocean Obs09: Sustained Ocean Observations and Information for Society*, vol. 2, p. 306, 2010.

[10] T. W. Research, "Ice abort handler," 2021. Accessed on May 1, 2024. [Online]. Available: https://datahost.webbresearch.com/viewtopic.php?f=3&t=455&p=1283&hilit=ice#p1283.

[11] Z. Duguid, "Towards basin-scale in-situ characterization of sea-ice using an autonomous underwater glider," Master's thesis, Massachusetts Institute of Technology, 2020.

[12] P. Ventola, G. Burgess, B. Claus, and R. Camilli, "An autonomous underwater glider with improved transport efficiency," *Journal of Oceanic Engineering*, in press.

[13] N. E. O. S. Data and I. S. (EOSDIS), "Nasa worldview," 2024. Accessed on May 1, 2024. [Online]. Available: https://worldview.earthdata.nasa.gov.

[14] U. MODIS Characterization Support Team (MCST). NASA MODIS Adaptive Processing System, Goddard Space Flight Center, "Modis 250m calibrated radiances product," 2017.

[15] Z. Duguid and R. Camilli, "Improving resource management for unattended observation of the marginal ice zone using autonomous underwater gliders," *Frontiers in Robotics and AI*, vol. 7, p. 579256, 2021.

[16] M. Wang, M. König, and N. Oppelt, "Partial shape recognition for sea ice motion retrieval in the marginal ice zone from sentinel-1 and sentinel-2," *Remote Sensing*, vol. 13, no. 21, p. 4473, 2021.